Developments in the Built Environment 24 (2025) 100812

Contents lists available at ScienceDirect

Developments in the Built Environment

journal homepage: www.sciencedirect.com/journal/developments-in-the-built-environment

From crack closure to durability improvement of cementitious mortar with knotted shape memory polymer (k-SMP) fibres

Tim Van Mullem [a], Nele De Belie [a], Riccardo Maddalena [b,*]

[a] Magnel-Vandepitte Laboratory, Department of Structural Engineering and Building Materials, Faculty of Engineering and Architecture, Ghent University, Technologiepark Zwijnaarde 60, B-9052 Gent, Belgium
[b] Cardiff University, School of Engineering, Cardiff, CF24 3AA, UK

ARTICLE INFO

Keywords:
Shape memory polymer
Crack closure
Self-healing
Water permeability
Chloride ingress
Carbonation

ABSTRACT

Extending the service life of concrete structures is increasingly important in the effort to reduce carbon emissions. Cracks compromise durability by accelerating degradation mechanism. Embedding shape memory polymer (SMP) fibres in cementitious materials offers a promising solution, as these fibres shrink upon thermal activation and induce crack closure. However, the influence of SMP fibre addition on the durability performance of cementitious materials has not yet been fully explored. In this study, knotted SMP fibres were embedded in mortar specimens, and durability was assessed through water flow testing, chloride diffusion, and carbonation measurements. Following thermal activation, SMP specimens achieved a perfect sealing efficiency, whereas water leakage persisted in reference samples, even after 14 days of wet/dry cycling. The reduced crack widths in the SMP specimens also limited the ingress of chloride ions and CO_2 at the crack location. Overall, the performance of the SMP series demonstrated a superior durability performance.

1. Introduction

Over the past decades significant efforts have been made to improve the carbon footprint of energy-intensive industries such as steel and concrete. The European Union is spearheading the sustainable transition by ways of the European Green Deal with the goal to have no net emissions of greenhouse gases by 2050 (European Commission). The building sector is a significant contributor to greenhouse gas emissions due to the usage of concrete and cement (Huang et al., 2018). In its net zero progress report the Global Cement Association lists the major contributors to achieve net zero as: carbon capture and utilisation/-storage (36 %), efficiency in design and construction (22 %), efficiency in concrete production (11 %), savings in cement clinker production (11 %), and savings in cement and binders usage (9 %) (Global Cement and Concrete Association, 2024). Thus, civil infrastructures' contractors and designers can contribute by increasing the efficiency in design and construction of concrete structures, which translates to re-use and service life extensions of concrete elements.

However, formation and propagation of cracks are one of the major factors hindering the concrete service life extension. They allow for a fast transport of liquid and gas into the concrete, resulting in the corrosion of the steel reinforcement and overall degradation. Aside from water, the ingress of chloride ions and CO_2 are two commonly known degradation mechanisms of concrete.

With regards to chloride attack, it has been established that both the width and the depth of the crack significantly influence the chloride ingress (De Schutter, 1999). Cracks wider than approximately 80–100 μm will act as an exposure surface (Jin et al., 2010; Gu et al., 2015), although there is some variation on the reported range which is depending on concrete properties and crack geometry. Very narrow cracks (smaller than 13–30 μm in width) do not influence the chloride ingress (Ismail et al., 2008; Yoon et al., 2010, 2014), and cracks with a width of 30–80 μm have an intermediate influence (Jin et al., 2010). When studying the influence of the crack depth, it was found that with an increasing crack depth the chloride penetration depth increases, while the distance between the chloride front and the crack tip decreases (Marsavina et al., 2009; Audenaert et al., 2009).

Similarly, several studies have highlighted that cracks allow for fast CO_2 ingress into the concrete (De Schutter, 1999; Alahmad et al., 2009; Ann et al., 2010; Song et al., 2006). Carević and Ignjatović (Carević et al., 2019) compared the critical crack width, i.e. the crack width below which there is no influence on carbonation depth, reported in different studies. This critical crack width lies around 8–10 μm (Alahmad et al., 2009; Torres et al., 2014; Zhang et al., 2011; Wang

* Corresponding author.
E-mail addresses: Tim.VanMullem@UGent.be (T. Van Mullem), MaddalenaR@cardiff.ac.uk (R. Maddalena).

https://doi.org/10.1016/j.dibe.2025.100812
Received 26 September 2025; Received in revised form 15 November 2025; Accepted 19 November 2025
Available online 20 November 2025

et al., 2018), although it is important to realize that smaller crack widths were not studied. For cracks with a width of 50 μm it has been reported that the carbonation depth was two-fold larger than that of uncracked samples, with the crack wall itself acting as an exposure surface (Carević et al., 2019).

Self-healing concrete has the ability to repair cracks, thereby delaying the fast ingress of water, CO_2, and deleterious ions into the concrete, which would otherwise trigger reinforcement corrosion and diminishing the service life. Many different types of self-healing technologies have been developed, and it has been proposed to group them into the following families: autogenous self-healing, stimulated autogenous self-healing (nonencapsulated), encapsulated autonomous self-healing, and self-healing bioconcrete (De Belie et al., 2018). A recent review work provided a comprehensive overview on the influence of crack geometry and size on degradation mechanisms of reinforced concrete, as well as the efficiency of different self-healing technologies in various aggressive exposure conditions (Cappellesso et al., 2023).

For example, it has been shown that the addition of superabsorbent polymers (SAPs) significantly reduced the chloride ingress into cracks compared to reference samples (Van Mullem et al., 2024). The addition of an organic-inorganic composite self-healing agent vastly improved the sealing efficiency (restoration of the water tightness) of cracked samples, as well reduced the impact of cracks on the chloride ingress (De Brabandere et al., 2024). In another study, cracked specimens with either a bacteria-based healing agent or with crystalline admixture were healed for three months in cyclic wet/dry condition (4 days wet/3 days dry) before submerging them up to one year in an artificial seawater solution (Cappellesso et al., 2024). For specimens with a narrow crack width (100 μm) the series with the bacterial healing agent obtained a chloride ingress reduction of 68 % at the location of the crack, while the series with the crystalline admixtures obtained a reduction of 32 %. When adding macrocapsules filled with a low viscosity polyurethane the self-healing efficiency was 75 % or higher in healed cracks from a depth of 6 mm onwards in chloride bulk diffusion testing (Van Belleghem et al., 2017), and even a consistent 100 % self-healing efficiency was recorded in a non-steady state chloride migration test (Van den Heede et al., 2018a). A more complete overview of the effect of self-healing on the chloride penetration resistance can be found in a recent article detailing how self-healing can be incorporated in design practices (He et al., 2025).

Studies on the influence of self-healing on the carbonation of cracked specimens are scarce. The studies that have been executed mostly use mortar samples in which part of the Portland cement was replaced by fly ash to reduce exposure times needed to obtain significant carbonation. One study found that adding macrocapsules filled with a low viscosity polyurethane resulted in five out of nine specimens behaving as if uncracked, i.e. the crack did not influence the carbonation front. When pressured macrocapsules (filled with the same polyurethane together with accelerator and benzoyl peroxide) were added, this even resulted in eight out of nine specimens having a carbonation front as if uncracked (Van den Heede et al., 2018b). The drawback of this study was that cracks were created by pulling thin metal plates out of the mortar after setting (which induced at the same time rupture of the capsules), which will have influenced the flow of the polyurethane out of the capsule. In a follow-up study cracks were induced via a crack width controlled three point bending test (Van Mullem et al., 2021). Specimens with macrocapsules filled with polyurethane had a carbonation depth at the location of the crack which was only half of that of the reference specimens. In another study, cracked samples with SAPs did not perform better regarding the carbonation front when compared to the reference samples, which was explained by an imperfect crack healing (Van Mullem, 2021).

Microfibres have also been used to stimulate autogenous and/or autonomous healing (De Belie et al., 2018), along with a beneficial crack-bridging effect. Snoeck et al. (2014) demonstrated that in mixtures containing synthetic microfibres, cracks as small as 30 μm could fully heal at the surface (crack mouth), regardless of whether superabsorbent polymers (SAPs) were present. However, in reference samples subjected to 28 days of wet/dry cycling, larger cracks up to 150 μm showed only partial healing, while for samples with SAPs a crack up to 138 μm was completely healed. Intrinsic self-healing capabilities have been demonstrated in fibre-reinforced cementitious composites, especially engineered cementitious composites (ECC). Characterised by a high volume of polymeric fibres, typically polyvinyl alcohol (PVA), polypropylene (PP) or polyvinyl ethylene terephthalates (PET), ECC can reduce crack widths to below 100 μm, a critical threshold for promoting autogenous healing through continued hydration and calcium carbonate precipitation (Yang et al., 2009). As such, the tight crack width in ECC not only reduces water permeability but also stimulates effective self-sealing, thereby restoring mechanical and transport properties after damage.

The inclusion of functional or smart fibres, such as steel, carbon, or shape memory alloy (SMA) fibres, can further enhance the self-healing efficacy by providing additional crack-closing forces by thermal activation features (Chen et al., 2021). Polymeric smart fibres with shape memory features have also been proposed as a self-healing technology. Shape memory polymers (SMP) are capable of undergoing large deformations and recovering their original shape upon exposure to an external stimulus such as heat, light, or moisture (Xie, 2011). Recent studies investigated the shape memory effect of PET-based materials in 3D and 4D printed composites (Ali et al., 2024; Rahmatabadi et al., 2024). When embedded in mortar or concrete, SMP fibres, strands or tendons can contract upon activation, inducing compressive stresses that close existing cracks, thus facilitating subsequent autogenous or autonomous healing processes (Teall et al., 2017; Maddalena et al., 2020). This mechanism allows for targeted and repeatable crack repair, which is scalable and especially beneficial for structures in aggressive environments (Davies et al., 2018). However, the integration of SMPs into cementitious matrices presents challenges in terms of compatibility, durability, and long-term performance, requiring careful consideration of polymer type, trigger mechanism, and matrix–interface behaviour (Maddalena et al., 2022). Hybrid systems combining smart reinforcement and SMP tendons also show potential, where pre-stress control microcracking and SMPs address wider or more localised damage zones (Balzano et al., 2021).

Previous work on k-SMP fibres mainly focused on visual crack closure at the crack mouth (Maddalena et al., 2020), and it was established in a cradle-to-gate life cycle assessment (LCA) that the addition of the k-SMP fibres resulted in a higher environmental impact compared to conventional concrete (Maddalena et al., 2022). However, this study did not consider the added functionality of crack closure and the resulting effects on durability and service life. In particular, the potential of SMP systems to enhance autogenous healing remains insufficiently explored. This work aims to address this gap by evaluating the extent to which SMP-induced crack closure can promote self-healing in mortar and enhance the durability, with a focus on chloride ingress and carbonation resistance.

2. Materials

Portland cement mortar specimens were used to test the effectiveness of crack closure. Tests were executed on two different groups: reference specimens without any shape memory polymer fibres, denoted “REF”, and specimens with shape memory polymer fibres, denoted “SMP”.

2.1. Knotted shape memory polymer (k-SMP) fibres

Knotted shape memory polymer (k-SMP) fibres with a diameter of 0.95 mm were manufactured from commercial grade polyethylene terephthalate (PET) with a tensile strength of 257 MPa (Maddalena et al., 2020). The manufacture process that provides the shape memory effect and characterisation of the fibre is described in previous work

(Maddalena et al., 2022). Fibres were cut and a single knot was manually made at each end. The knots provide mechanical anchorage for the fibres in the matrix so that both parts of a cracked specimen would be pulled together upon thermal activation (Maddalena et al., 2020). The distance between the knots was equal to a nominal length of 100 mm, which was ensured by using a 3D printed U-profile, see Fig. 1. Fibres were coated with demoulding oil prior to mortar casting to prevent bonding with the cementitious matrix which would inhibit the free shrinkage of the fibre upon thermal activation. Fibres were laid in the mortar mix aligned to the length of the mould.

2.2. Mortar composition and casting of specimens

All specimens were made with a mortar with a water-to-binder mass ratio of 0.55 and a sand-to-binder mass ratio of 3. The sand was sieved to a fraction 0–2 mm. The binder was made of Portland limestone cement CEM II A/L 32.5 R, with up to 20–25 % of limestone (Tarmac, UK, conforming to BS EN 197–1:2011), fly ash and silica fume. A total of 35 % wt. of the Portland limestone cement was replaced by fly ash (CEMEX, Fly ash 450-N, conforming to BS EN 450–1:2005) and silica fume (Elkem Microsilica, Norway), 30 % and 5 % respectively. Such mix design, with a residual content of Portland clinker of 45–48 %, was chosen to stimulate autogenous healing (Maddalena et al., 2021). For the REF series, without SMP fibres, polyvinylalcohol (PVA) fibres were added (MasterFiber 401, BASF, class Ia according to EN 14889–2:2006, equivalent diameter 0.12 mm, fibre length 12 mm, tensile strength 800 MPa). PVA fibres were chosen because their melting temperature (230 °C) was higher than the temperatures used in this study for SMP activation (150 °C), and because they showed to have a beneficial influence on the mechanical performance below 400 °C (Zhang et al., 2022). The dosage of PVA fibres was 2.1 % by weight of binder (which corresponds to approximately 10 kg/m^3 and 0.8 vol%). The SMP series were cast with the k-SMP fibres and no PVA fibres. A total of 30 k-SMP fibres were placed in each SMP specimen, corresponding to 0.83 vol%, calculated using the effective length of the fibres (100 mm). The dosage of the PVA fibres (or k-SMP fibres) was chosen to ensure an effective and stable crack creation, as a previous study (Maddalena et al., 2020) already established that plain mortar would fail at the crack widths of interest, see also section 3.1.

The cement, fly ash and silica fume were first dry mixed for 30 s, after which the mixing procedure according to EN196–1:2016 was followed. For the REF series, the PVA fibres were added in the mixing bowl before the last mixing step. This last mixing step, which describes mixing for 60 s at high speed, was lengthened to 90 s to ensure adequate dispersion of the PVA fibres. To ensure the same level of mixing energy, the same mixing procedure was followed for the SMP series. However, note that for the SMP series the k-SMP fibres were manually placed in the mould.

Specimens were cast in steel moulds (40 x 40 × 160 mm). For the series with k-SMP fibres, firstly, a mortar layer of ±5 mm was placed in the mould and compacted for 15 s on a vibration table. Then 10 oil-coated k-SMP fibres were placed in the centre of the moulds, ensuring a longitudinal alignment of the fibres, see Fig. 2a. A new layer of mortar (±5 mm) was then placed on top and vibrated for 15 s. The process continued until a total of 30 fibres were placed in the mould, after which the moulds were topped up with mortar and vibrated a final time for 25 s. Fig. 2b shows the schematic positioning of the 30 fibres in three layers of 10. For the REF series, the PVA fibres were placed directly in the mixer, however, the same mould filling procedure was followed to ensure the same level of compaction of the specimens.

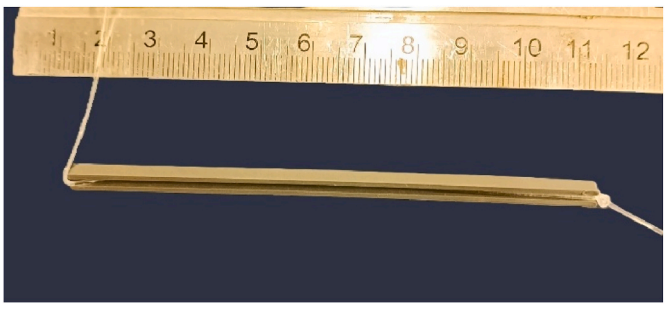

Fig. 1. Fibre knotting with U-profile to ensure effective length between the fibres of 100 mm (ruler in cm for scale).

After casting, moulds were wrapped with plastic foil and stored in laboratory conditions with no specific temperature control. The day after casting, specimens were demoulded and placed in a water curing tank at 20 °C.

3. Methods

The current experimental campaign was designed to assess any potential influence of k-SMP addition on durability. Aside from crack closure, water flow, chloride diffusion and carbonation were measured because the ingress of water, chloride ions or CO_2 are the source of degradation of concrete in many practical applications. Length changes were also recorded for calibration of future finite elements models, e.g. to study stress build-up upon thermal activation.

The experimental campaign considered different sets of specimens for each series (REF and SMP). The specimens were split up in sub-sets undergoing different treatments and measurements, as shown in Fig. 3. After crack induction (see section 3.1), specimens of **Set 1** were tested immediately after crack creation and k-SMP fibres' thermal activation, while specimens in **Set 2** underwent 14 days wet/dry (W/D) cycling prior to testing. The W/D cycles consisted of 1 h submerged in water, followed by 11 h drying at 20 °C and 60 % RH (relative humidity). Specimens were placed on their side face. Length changes were also measured on plain mortar specimens (denoted PM) which did not contain any type of fibres, see section 3.3.

3.1. Crack creation

A notch with a nominal depth of 2 mm was made at the bottom mid-span of all specimens using an electric saw, to ensure the exact location of the induced crack. Specimens were then cracked at an age of 14 days in a crack-width controlled three-point bending setup using crack mouth opening displacement (CMOD) control. Loading was stopped when the CMOD at the bottom of the specimens reached the target value of 350 μm for all specimens, except for the water flow testing specimens, for which one group of specimens was also cracked up to 500 μm.

3.2. Crack width measurement and k-SMP activation

Cracks were measured with a digital microscope with a 4K integrated camera (Keyence VHX-7000, Japan). The microscope was programmed to automatically acquire a stitched image of the crack mouth with a magnification of 80×. For each specimen an average crack width was calculated from 15 crack width measurements spaced over the length of the crack, following the recommendations by Round Robin Test 5 of the EU COST action SARCOS (Van Mullem et al., 2020a, 2020b).

After crack creation and acquiring a digital image, specimens were placed in an oven to activate the k-SMP fibres and induce crack-closure. Note that both the REF series (with PVA fibres and no shape memory effect) and the SMP series (with k-SMP fibres) underwent the thermal activation. This consisted of placing the specimens on their side in a pre-heated oven at 150 °C. After a duration of 3 h, specimens were removed from the oven and allowed to slowly cool to room temperature overnight, after which a new image of the cracked area was acquired.

3.3. Length changes

Following the procedure detailed in section 2.2 prismatic specimens

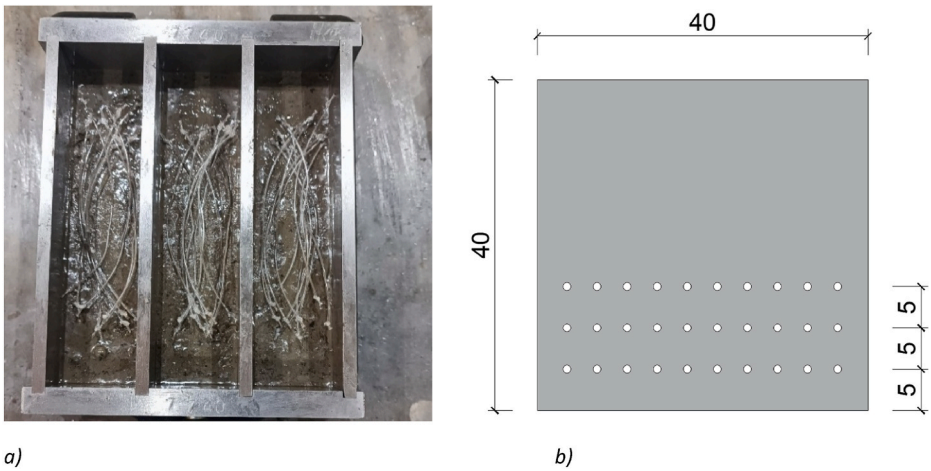

Fig. 2. a) Placement of knotted shape memory polymers on top of mortar layer, and b) sketch of cross-section of SMP specimen with 30 k-SMP fibres placed in layers of 10 (measurements in mm).

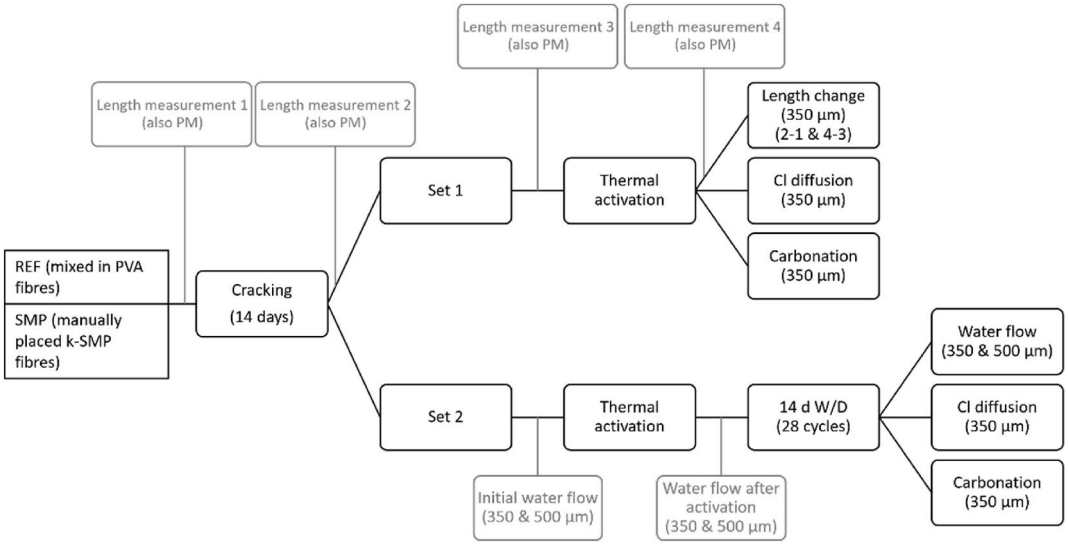

Fig. 3. Schematic overview of experimental plan. All tests were executed on REF and SMP specimens. Length measurements were also performed on PM specimens.

(40 x 40 × 160 mm) were made with cast-in stainless steel studs, one positioned at the centre of each end face (type 1 according to EN 12617-4, 2002). The length of the specimens was recorded with a digital gauge (accuracy 0.001 mm) at different stages: (1) before cracking, (2) immediately after cracking until 350 µm, (3) before thermal activation at 150 °C, and (4) 24 ± 2 h after removal from the oven. Based on these measurements, it was possible to calculate the macroscopic length changes due to cracking and thermal activation. As opposed to crack width measurements, this method also allowed to measure the strain changes in uncracked specimens, along with possible drying shrinkage effects. Measurements were conducted on one uncracked and three cracked specimens of both REF and SMP series. In addition, also the length of three PM specimens, made of plain mortar without any type of fibres, was measured. These PM specimens remained uncracked, as it was already mentioned that plain mortar specimens would fail at the crack widths of interest (Maddalena et al., 2020).

3.4. Water flow testing

A water permeability test was used to assess the effect of crack closure and subsequent self-healing (Tziviloglou et al., 2014, 2016; Gruyaert et al., 2016). The prismatic specimens (40 x 40 × 160 mm) were made in moulds which have an opening centrally positioned at the end faces. The moulds were filled following the procedure described in section 2.2. When the final layer of 10 k-SMP fibres was placed, round steel bars (⌀ 3.5 mm) were put through the openings, see Fig. 4a. These bars were oil-coated to ease their pull-out upon demoulding, leaving a hollow channel along the specimens, see Fig. 4b.

Eight specimens were prepared for both the REF and SMP series; four were cracked up to 350 µm and the other four were cracked until 500 µm. Prior to cracking, the opening at one end face was enlarged via mechanical drilling over a length of 20 mm to allow the insertion of a tube ($\varnothing_{out} = 6$ mm, $\varnothing_{in} = 4$ mm). A watertight connection was ensured via an all-weather co-polymer sealant and Teflon tape. The opening on the other end face was closed off with the sealant.

After crack creation, specimens were saturated overnight in deionised water. A water permeability test (Tziviloglou et al., 2014, 2016; Gruyaert et al., 2016) was executed by connecting the tube inserted in the specimen to a tube ($\varnothing_{out} = 5$ mm, $\varnothing_{in} = 8$ mm) connected with a water reservoir. The water height was kept constant at 500 ± 20 mm. Water flowed from the reservoir via the tubing into the cast-in hole, from where it could leak from the crack. After the flow had stabilised, the water was captured in a container placed on a scale during a period of at least 5 min. To improve accuracy, the period was longer for small flow

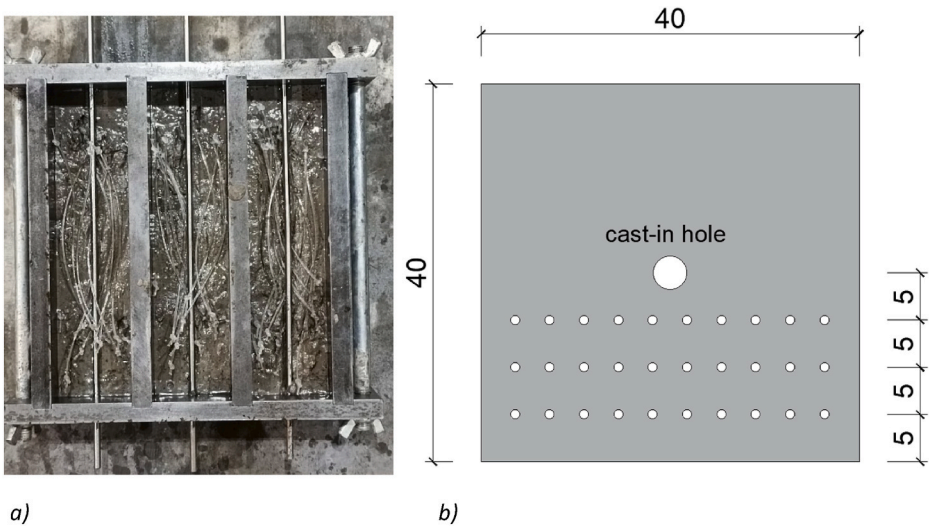

Fig. 4. a) Casting of SMP samples with placement of an oiled steel rod for water flow testing, and b) sketch of cross-section of SMP specimen with cast-in hole (after removal of steel rod) (measurements in mm).

rates: at least 10 min for a flow rate smaller than 10 g/min and at least 15 min for a flow rate smaller than 3.5 g/min.

After the initial water permeability test, specimens were placed in the oven for thermal activation. After allowing the specimens to cool to room temperature overnight, the crack closure was recorded by using the digital microscope and the specimens were saturated overnight prior to performing a subsequent permeability test.

To test the effect of stimulated autogenous healing, specimens then were placed on their side face in a wet/dry chamber (1 h wet and 11 h dry) for 14 days. At 7 and 14 days a new water permeability test was executed to record the sealing efficiency.

3.5. Chloride diffusion

Prior to chloride exposure, all sides of the prismatic specimens were coated with one layer of two-part epoxy, except for the exposure surface, i.e. the bottom surface where the crack mouth was located. After curing of the epoxy, the specimens were first saturated in deionised water for 2 days, then positioned on their side face and submerged into a 3.3 % wt. NaCl solution at room temperature. This concentration of NaCl is comparable to the one of sea water. The ratio of exposure surface over volume of NaCl solution was constant and equal to 42 cm^2/dm^3. After 1 and 4 weeks, minimum three REF and three SMP specimens of **Set 1** and **Set 2** were removed from the solution. Two REF and two SMP samples of **Set 2** were removed from the NaCl solution after 15 weeks. Specimens were dried for 24 h in uncontrolled laboratory conditions to prevent liquid in the crack from influencing the chloride profile when splitting the samples. Specimens were then split longitudinally perpendicular to the direction of the crack, and the chloride penetration depth was identified by the colorimetric method, using a 0.1 M silver nitrate solution (Kim et al., 2013). The depth of the colour change boundary was determined at 0, 2, 4, 8, 12, 16, 20, 30, 40, 50 and 60 mm away from the crack.

3.6. Carbonation

For the set of specimens which did not undergo prior W/D cycling (**Set 1**), and for the set which did undergo W/D cycling (**Set 2**), samples were pre-conditioned either immediately after thermal activation or after W/D cycling. EN 12390-12, 2020 prescribes conditioning specimens for 14 days in a laboratory air environment. This was adapted due to time constraints. Specimens were oven-dried for 24 h at 40 °C, followed by 6 days conditioning in laboratory air environment, in order to get a homogenous moisture distribution. Specimens were then sealed with aluminium tape, except for the exposure surface, i.e. the bottom surface where the crack mouth was located. Samples were placed on their side face in a carbonation chamber (FDM, Italy) with a 3 % CO_2 concentration (as described by EN 12390-12, 2020) and at 20 °C and 60 % RH. After 1 and 4 weeks, minimum three REF and three SMP specimens of **Set 1** and **Set 2** were removed from the chamber. Two REF and two SMP samples of **Set 2** were removed from the chamber after 15 weeks. Specimens were split longitudinally perpendicular to the crack, and the carbonation front was identified by spraying a 1 % phenolphthalein solution. Similar as for the chloride diffusion test, the depth of the colour change boundary was determined at 0, 2, 4, 8, 12, 16, 20, 30, 40, 50 and 60 mm away from the crack.

4. Results and discussion

4.1. Flexural and compressive strength

Flexural and compressive strength values of REF, SMP and PM mixes as a function of age (14, 28, 56 and 91 days) are reported in Figs. 5 and 6, respectively. Tests were performed on mortar prisms (40 x 40 × 160 mm) according to EN 196-1, 2016. Whilst series, REF, SMP and PM were cast with the same mortar composition (see section 2.2), the

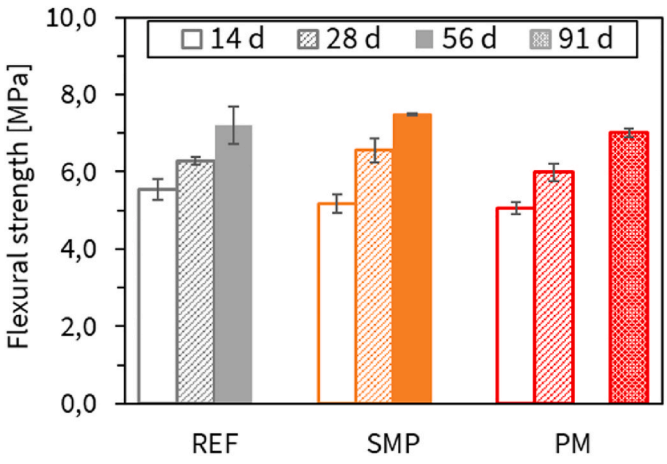

Fig. 5. Flexural strength at the age of 14, 28, 56 and 91 days of the REF, SMP and PM series. Error bars represent the standard deviation (n = 3).

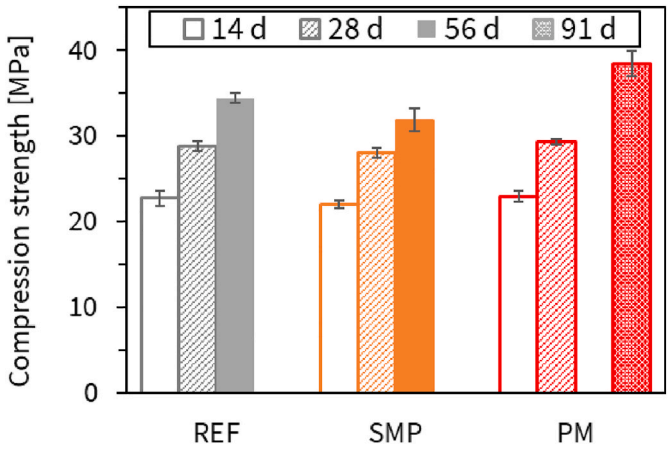

Fig. 6. Compression strength at the age of 14, 28, 56 and 91 days of the REF, SMP and PM series. Error bars represent the standard deviation (n = 6).

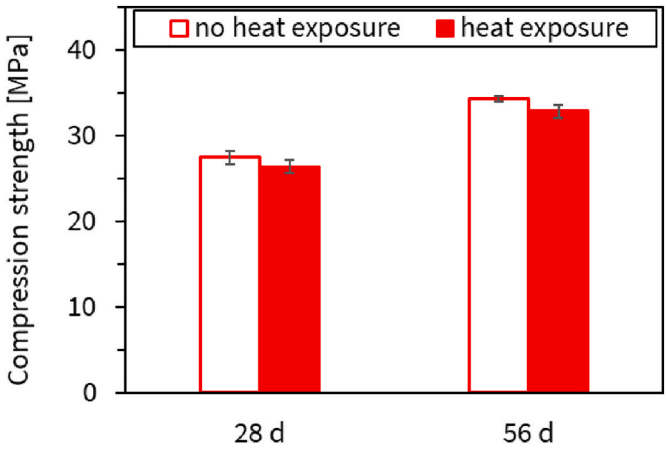

Fig. 7. Comparison of compression strength of PM specimens which underwent a heat exposure and specimens which did not. Error bars represent the standard deviation (n = 6).

REF series included PVA fibres, the SMP series had manually placed k-SMP fibres, and the PM series had no fibres. Note that no strength measurements were done on the PM series at 56 days, but instead strength measurements were done at 91 days.

With regards to the flexural strength (Fig. 5) the fibres resulted in a slightly improved flexural strength: the REF series was 10 % (14 days), and 5 % (28 days) stronger than the PM series, while the SMP series was 2 % (14 days), and 9 % (28 days) stronger than the PM series. The clear benefit of the fibres, i.e. the crack bridging effect which allows to take up tensile forces, is only achieved after crack initiation. The test program to determine the flexural strength stopped when a crack was first detected, thus this effect is not captured in this test.

The compressive strength (Fig. 6) of both series with fibres (REF and SMP) was comparable to that of the PM series: the REF series was 1 % (14 days), and 2 % (28 days) weaker than the PM series, while the SMP series was 4 % (14 days and 28 days) weaker than the PM series. A comparison at 56 days was not possible as it was decided to test the PM series at 91 days in order to demonstrate the long-term strength development resulting from the high degree of Portland cement replacement. From 28 to 91 days the strength of the PM series increased by 31 %.

A control test was executed to determine whether the thermal activation step (see section 3.2) had an influence on the strength development, i.e. whether the water loss during the heat exposure negatively impacted the overall strength. To this end two PM batches of mortar prisms (40 x 40 × 160 mm) were cast. At an age of 14 days the specimens were removed from the curing tank. After 24 h half of them underwent the same heat exposure used for SMP thermal activation (3 h at 150 °C), whilst the other half remained at laboratory conditions. All specimens were left overnight at laboratory conditions and were then placed back in a curing tank. Strength tests were performed at an age of 28 and 56 days. Fig. 7 shows the compressive strength of the specimens that underwent heat exposure compared to those that did not. The strength for the specimens that underwent heat exposure was on average slightly lower. An independent sample *t*-test showed a statistical difference of the means (level of significance = 5 %, *p* - value (28 days) = 4.9 %, *p* - value (56 days) = 0.1 %). Nevertheless, it is important to realize that the strength for the series exposed to heat is only 4 % lower (both for 28 days and 56 days) which is relatively smaller than the strength gain with age (125 % for the set which did not undergo heat exposure and 124 % for the set which did undergo heat exposure). Hence, it can be concluded that the heat exposure did influence the hydration process, yet minimally.

4.2. Crack width and crack closure

The crack width was measured before and after thermal activation of the k-SMP fibres. Fig. 8 shows the average crack width of the specimens used for water flow testing and shrinkage measurements. The specimens for water flow testing consisted of two groups: one group cracked up until a CMOD reading of 350 μm was achieved, and the other cracked up until a CMOD reading of 500 μm. The specimens for shrinkage measurements were cracked up until a CMOD reading of 350 μm.

For specimens cracked to 350 μm prior to thermal activation, shrinkage specimens exhibited slightly larger crack widths than water flow specimens. The latter contained a cast-in hole —a void on the crack wall— likely reducing resistance upon unloading due to lower wall roughness. Across all groups, SMP specimens showed markedly lower crack widths than their REF counterparts before thermal activation, attributable to PET fibre–induced elastic crack closure. For SMP specimens cracked to 350 μm, the average elastic closure was equal to 289 μm (water flow) and 262 μm (shrinkage), increasing to 409 μm for those cracked to 500 μm. Values were obtained by subtracting the microscope-measured crack width from the CMOD at unloading (350 or 500 μm). In contrast, REF specimens exhibited closures of 201 μm (water flow) and 191 μm (shrinkage) when cracked to 350 μm, and 270 μm when cracked to 500 μm.

Following thermal activation, both REF and SMP series exhibited substantial crack closure. Comparing crack widths before and after activation showed closures of 35 % (water flow - 500 μm) and 38 % (water flow - 350 μm; shrinkage - 350 μm) for the three REF series. In contrast, the SMP series achieved markedly higher closures of 83 % across all groups, despite having smaller pre-activation crack widths.

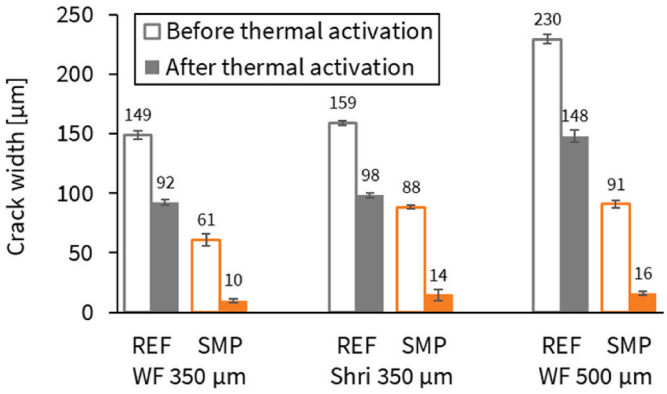

Fig. 8. Average crack width of water flow (WF) and shrinkage (Shri) specimens before and after thermal activation. Error bars represent the standard error on the mean (n = 4 for water flow specimens, n = 3 for shrinkage specimens).

Post-activation, SMP specimens had average crack widths of only 10–16 μm. This high closure efficiency is attributed to heat-triggered recovery of the PET fibres' shape memory, enabling them to retract towards their pre-cracked state.

Literature reports that PVA fibres, present in the REF mix, undergo a diameter reduction when embedded in cementitious matrices and heated to 200 °C due to thermal degradation, leading to bond loss with the matrix (Wang et al., 2020). Consequently, PVA fibres are unlikely to have contributed significantly to crack closure in REF specimens. Instead, closure in the REF series likely resulted from matrix shrinkage induced by free-water loss during heat exposure. The SMP series likely experienced similar shrinkage but benefited additionally from the active crack-closing effect of the PET fibres' shape memory response.

4.3. Length changes

The length of the shrinkage specimens was measured before and after cracking, as well as prior to thermal activation and 24 ± 2 h after removal from the oven. From these measurements the strain change was calculated. The results are presented in Fig. 9. Because the length was measured centrally along the cross-section, the values are correlated to the crack width (measured at the crack mouth) but cannot be directly translated. Nevertheless, these measurements might provide a basis for future research, e.g. to calibrate models to estimate the stress build up in the cementitious matrix during thermal activation of the shape memory polymers.

For the REF and SMP series, Fig. 9 shows the average strain change of three specimens cracked to 350 μm, as well as the strain change of one uncracked (UNCR) control specimen. For the PM series, all three specimens remained uncracked. First, for specimens cracked to 350 μm, the strain change in the REF series is approximately twice that of the SMP series. This corresponds to the crack width measurements executed prior to thermal activation (see section 4.2); the crack width of the SMP specimens for shrinkage measurements was on average only 55 % of the REF shrinkage series. The elastic closure observed can be attributed to the PET fibres, which continue to contract after unloading, progressively narrowing the crack width (Teall et al., 2017; Maddalena et al., 2020). For the uncracked specimens a small shrinkage was measured likely due to water evaporation (specimens were surface dry for cracking but were cured in saturation tanks).

After thermal activation, the uncracked SMP specimen showed a slightly greater strain change (−235 μm/m) compared to the PM series (−211 μm/m). The uncracked REF specimen exhibited a markedly higher shrinkage (−523 μm/m), although it should be noted that this value is based on a single specimen. For the cracked specimens, thermal activation resulted in greater shrinkage in the REF series than in the SMP series, although crack width closure was slightly larger in the SMP specimens (74 μm) compared with the REF specimens (61 μm). This difference can be explained by the higher nominal volume of hardened cementitious matrix in the REF specimens, which is more prone to water evaporation and subsequent drying shrinkage. In contrast, the bulky knots of the SMP fibres, not accounted in the total volume dosage, occupy part of the matrix volume, reducing the amount of cementitious material available to shrink. The presence of PVA fibres might also increase porosity in the interfacial transition zone and, consequently, the amount of evaporable water, thereby contributing to shrinkage upon drying (Tran et al., 2022; He et al., 2023).

4.4. Water flow

Before thermal activation a water flow test was performed. The initial flow rate which was obtained is shown in Fig. 10. For the REF series, the two groups cracked to nominal widths of 350 μm and 500 μm, respectively, are clearly distinct. In the SMP series, the values are much closer, which can be explained by the small difference —only 30 μm— between the average residual crack widths after unloading of the 350 μm and 500 μm groups. All specimens in the SMP series obtained a flow rate smaller than 1 g/min, except for one specimen with an average crack width of 94 μm which showed a flow rate of 1.1 g/min. This outcome is expected, as water ingress occurred through the centrally positioned cast-in hole, resulting in a local crack width considerably smaller than the average crack width at the crack mouth reported in section 4.2. Assuming a linear reduction in crack width from the crack mouth (measured to be 61 μm for specimens cracked to 350 μm and 91 μm for specimens cracked to 500 μm, see section 4.2) to zero at the top of the specimen, the estimated average local crack widths at the cast-in hole are 35 μm and 52 μm for the SMP specimens cracked to 350 μm and 500 μm, respectively. The actual values are likely lower, as the crack tip is unlikely to extend over the full specimen height. Such narrow effective crack widths are well within the threshold for autogenous healing through carbonation and continued hydration, suggesting favourable conditions for self-sealing in these specimens. Furthermore, given their larger diameter and total volume per specimen, compared with PVA fibres, k-SMP fibres may have more effectively restricted, or even blocked the water flow. For the specimens in the REF series the effective crack width was larger, and the much smaller PVA fibres did not provide a significant crack blocking compared to the k-SMP fibres, resulting in an average flow rate of 5.4 g/min and 18.2 g/min, for the specimens cracked until 350 and 500 μm respectively.

After thermal activation, a second water flow test was performed. Subsequently, specimens were placed in W/D cycling, and the flow rate was determined after 7 and 14 days. The obtained flow rate q_i at a given time i was compared to the initial flow rate $q_{init.}$ by calculation of the sealing efficiency SE for each individual sample, see equation (1):

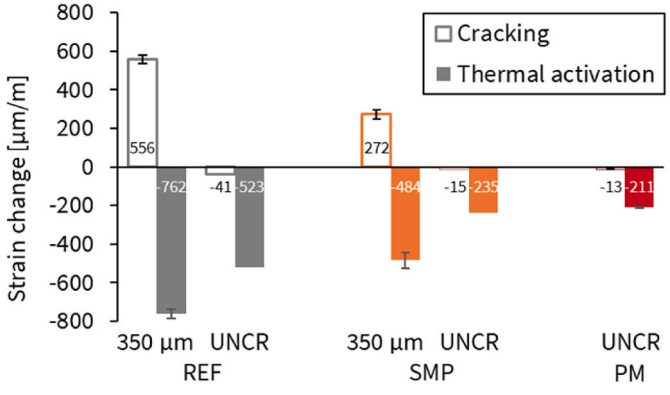

Fig. 9. Macroscopic strain changes due to cracking and thermal activation respectively. Error bars represent the standard error on the mean (n = 3, except for REF UNCR and SMP UNCR for which n = 1).

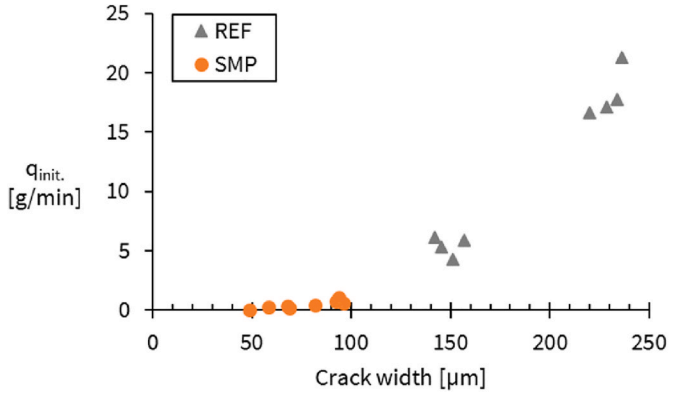

Fig. 10. Initial flow rate $q_{init.}$ (before thermal activation) as function of the nominal crack width for specimens cracked until 350 and 500 μm.

$$SE = \frac{q_{init.} - q_i}{q_{init.}} \quad \text{Eq. 1}$$

Specimens were saturated prior to flow testing. The average sealing efficiency is shown in Fig. 11. The REF specimens have a relatively high sealing efficiency after the thermal activation (on average 82 % for the 350 μm specimens and 77 % for the 500 μm specimens). However, after W/D cycling the sealing efficiency did not improve significantly. This indicates a negligible autogenous crack healing. Previous results from the authors indicated a significant sealing by autogenous healing for reference mortars made with CEM I (SE = 48.9 % by healing for 14 W/D cycles (12 h wet/12 h dry), and SE = 93.6 % for 28 W/D cycles, with specimen orientation not specified (Van Mullem et al. 2019)). In the current study, a CEM II binder was used instead, of which part was replaced by fly ash and silica fume. Possibly, the short healing period has prevented the full reaction of the supplementary cementitious materials. To verify this, specimens were kept for a prolonged time (more than 140 days) in W/D cycles. Microscope images of the crack area did not show significant formation of healing products, see Fig. 12. This may be due to the high Si/Ca ratio of the binder system (CEM II + fly ash + silica fume), potentially limiting the availability of calcium hydroxide (Hamada et al., 2023) to sustain the pozzolanic reaction and form additional hydration products in the cementitious matrix; however, this explanation is speculative. Another possible explanation for the lack of deposited healing products might be the specimens' orientation during W/D cycling (specimens were stored on their side face). A study on bacterial concrete showed that the best visual crack closure was obtained for cracks oriented downwards during W/D cycling, as gravity and water movement tend to deposit healing products at the crack mouth (Van Mullem et al., 2020c). A recent study using micro-computed tomography also concluded that healing efficiencies calculated from crack width measurements or water flow testing do not necessarily correlate with volume changes in the internal volume of the crack (Grosso Giordano et al., 2024). Even though healing was not observed with the current binder system, specimen orientation and healing environment, the reduced crack widths which were measured, would contribute to autogenous healing (Mihashi et al., 2012; De Rooij et al., 2013).

For the SMP series, all specimens showed a perfect sealing efficiency. Since both after thermal activation and 7 days W/D cycling no water flow was detected, the specimens were not tested again after 14 days W/D cycling. The relatively narrow crack width (see section 4.2) combined with crack blocking by the k-SMP fibres resulted in a consistent 100 % sealing efficiency of all SMP specimens (both the 350 μm and 500 μm specimens).

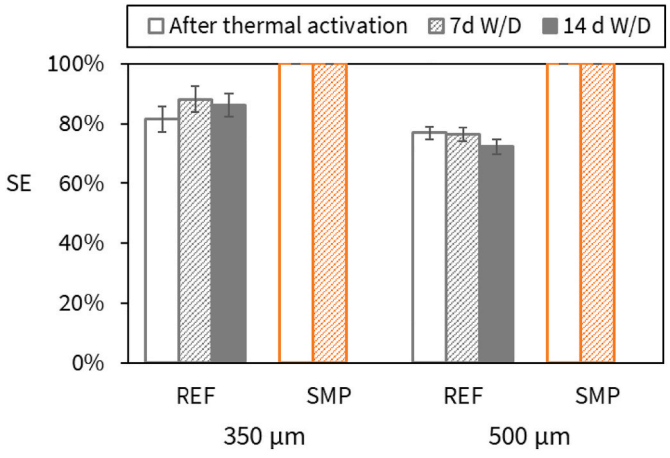

Fig. 11. Average sealing efficiency *SE* calculated after thermal activation after 7 days of W/D cycling and after 14 days of W/D cycling. Error bars represent the standard error on the mean (n = 4).

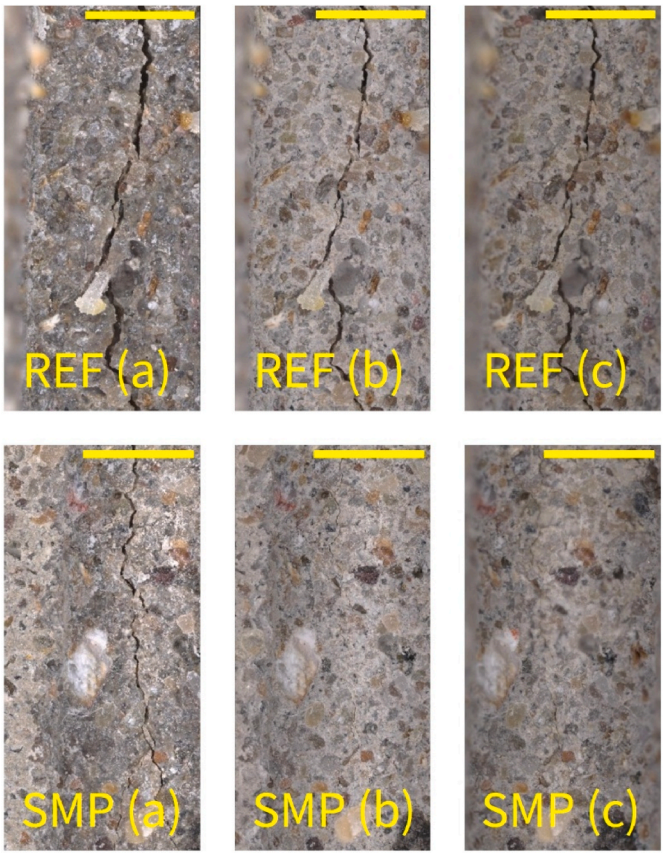

Fig. 12. Microscope images at the crack mouth of a representative REF and SMP specimen: (a) before thermal activation, (b) after thermal activation, (c) after more than 140 days of W/D cycling (scale bar = 20 mm).

Based on these results it is expected that even larger crack widths can be sealed by combining k-SMP fibres with a tailored binder system that promotes autogenous healing at microstructure level.

4.5. Chloride diffusion

Specimens of **Set 1** were saturated in deionised water for 2 days and then saturated in a 3 % wt. NaCl solution immediately after thermal activation. Fig. 13 shows the depth of the colour change boundary after spraying with silver nitrate. The averages are in general based on triplicates, but for some locations only two measurements were available.

Fig. 13 shows that the crack is the preferential ingress path for the chloride ions, which is evident from the peak at a zero perpendicular distance to the crack. After 7 days of submersion in a chloride solution, the ingress in both series is comparable. After 28 days, chloride ions have penetrated significantly deeper into the cracks of the REF samples ($p_{one-sided}$ = 0.2 %, level of significance = 5 %). The depth of chloride ingress into the crack is on average 15 % lower in the SMP series. Comparing the depth of ingress in the uncracked area of the same samples (i.e. approximately 20 mm away from the crack where the ingress depth becomes constant) there is no difference between the REF and SMP samples, due to the same cementitious matrix. Between 7 and 28 days of submersion, chlorides penetrated deeper in the uncracked zone. Surprisingly, the depth of ingress in the cracked zone was lower after 28 days, which may be attributed to variability in crack geometry because the 7- and 28-days measurements were made on different specimens.

After thermal activation, specimens of **Set 2** were first subjected to W/D cycling for 14 days and then were immersed in the chloride solution following a 2-day pre-saturation in deionised water. Fig. 14 shows

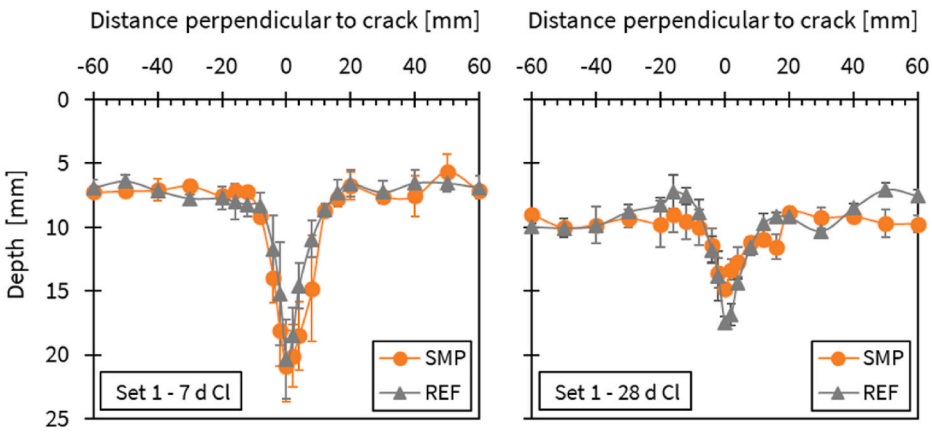

Fig. 13. Depth of the $AgNO_3$ colour change boundary of Set 1 specimens, which did not undergo W/D cycling prior to submersion in a chloride solution for 7 days (left) and 28 days (right). Error bars represent the standard error on the mean (n = 3).

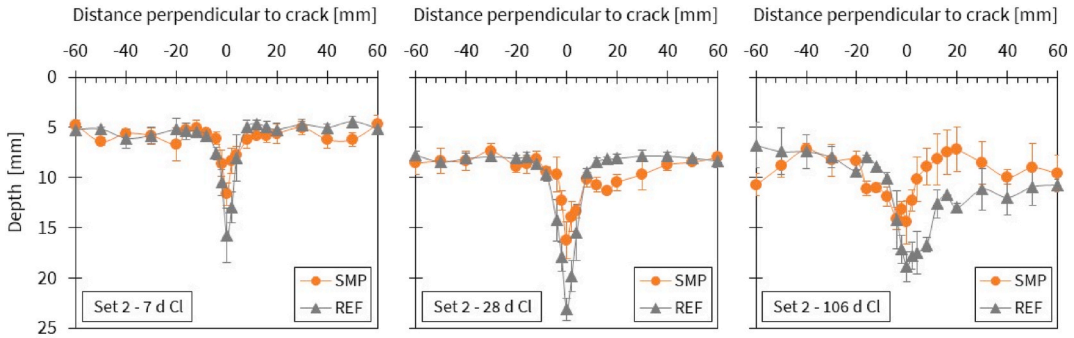

Fig. 14. Depth of the $AgNO_3$ colour change boundary of Set 2 specimens, which underwent W/D cycling prior to submersion in chloride solution for 7 days (left), 28 days (centre) and 106 days (right). Error bars represent the standard error on the mean (n = 3, except for REF 28 days specimens for which n = 4 and for the REF and SMP 106 days specimens for which n = 2).

the depth of the colour change boundary. Note that the results of 106 days are based on duplicates, instead of triplicates. This might partially explain the high variability on these specific measurements. In addition, variability on crack geometry, crack healing and crack width can compound as the exposure progresses.

Fig. 14 shows that the chlorides have consistently penetrated deeper in the cracked zone of the REF samples. Although it needs to be mentioned that at 7 days the deeper average ingress of the REF samples is the result of one single specimen, showcasing an 8 mm deeper ingress in its crack compared to the other two samples of the series. As an example, after 28 days of chloride exposure there is a statistical difference with a *p*-value of 1.9 % (level of significance = 5 %). The average chloride ingress at the location of the crack for the SMP series is 26 %, 30 %, and 23 % lower compared to the REF series, respectively for 7, 28 and 106 days.

As mentioned in the introduction, very narrow cracks (smaller than 13–30 μm) do not influence the chloride ingress (Ismail et al., 2008; Yoon et al., 2010, 2014), while wider cracks (80–100 μm) act as an exposure surface (Jin et al., 2010; Gu et al., 2015) and intermediate cracks (30–80 μm) show a transitional influence (Jin et al., 2010). The dependency of the chloride ingress on the crack width for narrower cracks explains the better performance of the SMP samples. For **Set 2** there is potential autogenous healing (due to W/D cycling) which is more effective in narrow cracks (Snoeck et al., 2015).

4.6. Carbonation

After thermal activation and pre-conditioning, specimens of **Set 1** were placed immediately in the carbonation chamber. At the given time, the carbonation depth was measured using the colorimetric method previously described. Fig. 15 shows the depth of the carbonation front. The averaged values are based on triplicates, except for the cracked region of the 7 days SMP specimens for which the measurements of one specimen were deemed unreliable and discarded, due to severe fractures around the crack resulting from splitting the specimen.

Similar as for the chloride diffusion specimens, the carbonation front is deeper at the location of the crack. After 7 days in the carbonation chamber the carbonation fronts of SMP and REF samples are similar to each other. However, after 28 days, a clear difference emerged in the average depth of the carbonation front at the crack location ($p < 0.01$ %, level of significance = 5 %), where the carbonation front is 24 % less deep in the SMP series when compared to the REF series.

Specimens of **Set 2** were first subjected to W/D cycling for 14 days after thermal activation, and then pre-conditioned prior to CO_2 exposure. Note that the averaged values plotted for 105 days exposure in the carbonation chamber are based on duplicates instead of triplicates. The 28-day average for the SMP series at 40 and 50 mm from the right-hand side of the crack is based on a single result due to excessive damage at that location from splitting the samples. There is a clear difference between the REF and SMP series at the location of the crack ($p_{7\ days} = 1.1$ %, $p_{28\ days} = 0.7$ %, level of significance = 5 %). The SMP series performed consistently better than the reference. The average carbonation front at the location of the cracks of the SMP series is 37 % and 38 % less deep compared to the REF series after 7 and 28 days of exposure respectively. Note that after 105 days of exposure the carbonation front reached the full height of the REF specimens (40 mm), while it was only 29 mm deep in the SMP series. Hence, a quantitative comparison for 105 days of exposure is not possible. Nevertheless, these

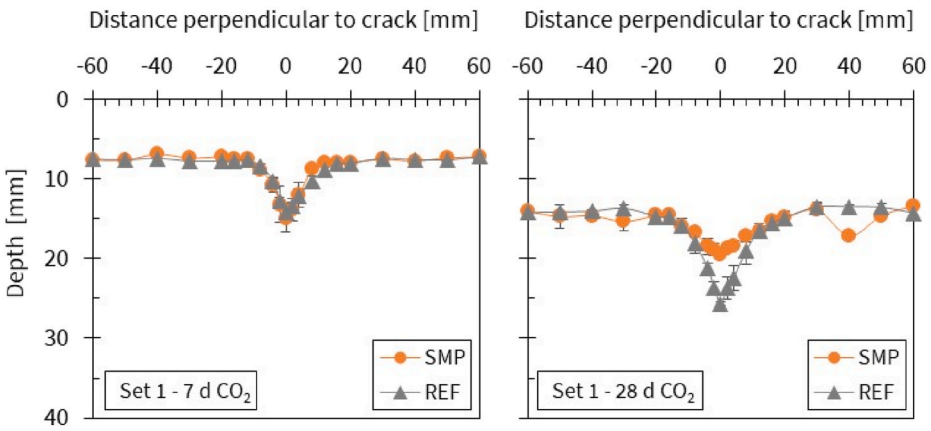

Fig. 15. Depth of the phenolphthalein colour change boundary of Set 1 specimens, which did not undergo W/D cycling prior to exposure in a carbonation chamber for 7 days (left) and 28 days (right). Error bars represent the standard error on the mean (n = 3, except for the cracked zone of the 7 days SMP specimens for which n = 2).

Table 1
Ratio of the carbonation depth in the crack over the average depth in the uncracked zone (* quantitative calculation not possible because the carbonation front in the crack reached the full height of the specimens).

	Set 1		Set 2	
	REF	SMP	REF	SMP
7 days	189 ± 18 %	199 ± 47 %	356 ± 48 %	319 ± 40 %
28 days	185 ± 3 %	133 ± 3 %	318 ± 40 %	180 ± 31 %
105 days	–	–	*	127 ± 7 %

results suggest that, in addition to the carbonation front being shallower in the cracks of the SMP samples, the width of the affected zone due to the presence of the cracks is also reduced.

Table 1 presents the average ratio of the carbonation front depth at the crack location to that in the uncracked zone (measured >20 mm away from the crack), which was calculated for each specimen. A value of 100 % indicates equal carbonation depth in both the crack and the uncracked zone. As the exposure period increases, this ratio drops significantly for the SMP series—regardless of the set—while it remains more constant for the REF series. Previous studies have reported that carbonation in cracked cementitious materials depends on crack width, crack depth, and crack geometry (De Schutter, 1999; Van Mullem et al., 2020d). Alahmad et al. (2009) found that for cracks wider than 60 μm, the carbonation depth perpendicular to the crack wall is equivalent to that from the exposed surface. The progressive ratio drop observed in the SMP samples can therefore be explained by the gradual reduction in crack width as the carbonation front advances; narrowing, rough crack walls increasingly restrict CO_2 ingress. In **Set 2** specimens partial crack healing also possibly reduced crack connectivity, further limiting carbonation. This highlights the SMP series' enhanced ability to slow carbonation ingress through active crack closure, in contrast to the REF series, where wider cracks maintained more direct pathways for CO_2 penetration.

The ratio of carbonation depth at the crack to that in the uncracked zone was higher for **Set 2** specimens (see Table 1). Part of the binder was replaced with supplementary cementitious materials, meaning specimens had not reached full maturity at the time of cracking. Consequently, **Set 2** specimens likely benefitted from additional curing during the W/D cycles, which promoted further hydration and refinement of the microstructure. This resulted in a lower carbonation depth in the uncracked zone compared with **Set 1** specimens (Figs. 15 and 16) and, therefore, a higher relative difference with the carbonation depth at the crack.

It should be noted that issues with the humidifier unit in the carbonation chamber caused fluctuations in environmental conditions. Caution is therefore advised when comparing these results with other studies. Nevertheless, both REF and SMP specimens within a given set entered the chamber simultaneously and were exposed to identical conditions throughout the test period.

5. Conclusion

Shape memory polymer (SMP) PET fibres with a single knot at the outer ends (to improve anchorage with the cementitious matrix) were pre-placed in prismatic moulds when casting mortar specimens. Thermal activation after cracking of the specimens triggered recovery of the

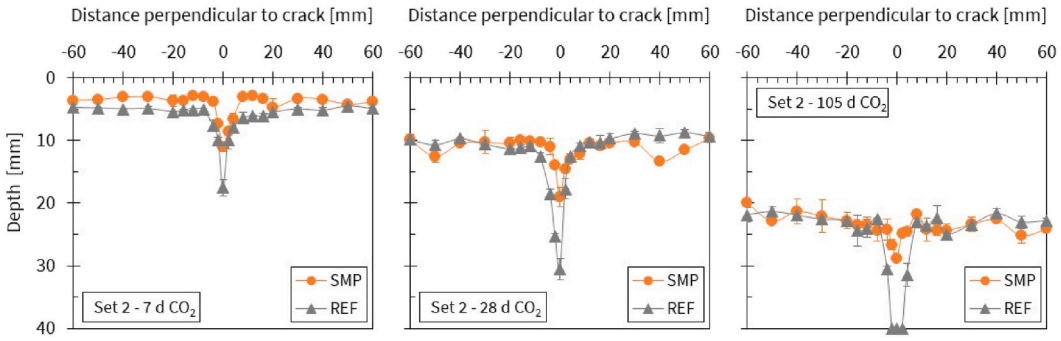

Fig. 16. Depth of the phenolphthalein colour change boundary of Set 2 specimens, which underwent W/D cycling prior to exposure in a carbonation chamber for 7 days (left), 28 days (centre) and 105 days (right).Error bars represent the standard error on the mean (n = 3, except for the REF and SMP 105 days specimens for which n = 2).

fibres' shape memory resulting in crack closure. The following conclusions with regards to the self-healing and durability performance can be drawn:

- The thermal activation only had a marginal influence on the hydration process as evidenced by a slightly lower compressive strength compared to a control series with ideal curing.
- For specimens cracked up until a CMOD reading of 350 μm, the SMP fibres induced a significant elastic crack closure of more than 75 %. After thermal activation there was an additional crack closure of 83 %, resulting in a final average crack width smaller than 15 μm.
- After thermal activation, no water leakage was recorded from the cracked SMP specimens in the water flow test; in other words, a consistent 100 % sealing efficiency was obtained.
- The narrower cracks of SMP specimens compared to REF specimens partially restricted chloride diffusion into the crack. The depth of the colour change boundary was 23 % (testing period of 106 days) to 30 % (28 days) lower for the set subjected to W/D cycling for 14 days.
- The carbonation front at the crack location was less deep for the SMP specimens compared to REF specimens. Furthermore, as the exposure period increased, the influence of the crack on the carbonation front decreased for the SMP specimens which can be attributed to the small crack widths. In contrast, for the REF specimens the influence of the crack remained dominant.

The overall better performance of the SMP series was linked to narrower crack widths. The durability performance might be further increased in future research by using a binder system with a higher autogenous healing potential. Additional investigation should be carried out to assess the efficiency of repeated crack opening and subsequent SMP activation, in combination with potential formation of stress-recovery induced microcracks resulting from the cyclic action.

CRediT authorship contribution statement

Tim Van Mullem: Conceptualization, Data curation, Formal analysis, Funding acquisition, Investigation, Methodology, Project administration, Validation, Visualization, Writing – original draft. **Nele De Belie:** Funding acquisition, Writing – review & editing. **Riccardo Maddalena:** Funding acquisition, Methodology, Resources, Writing – review & editing.

Declaration of competing interest

The authors declare that they have no known competing financial interests or personal relationships that could have appeared to influence the work reported in this paper.

Acknowledgement

This research was supported by a travel grant awarded by the fwo (Research Foundation –Flanders). Yasmina Shields is thanked for supplying the U-shaped profiles used for fibre knotting. The EPSRC-funded Resilient Materials 4 Life (RM4L) Life (RM4L) grant is acknowledged. The technical staff of the Resilient Construction Materials and Structures Laboratories of Cardiff University (UK) are recognised for their support in carrying out the experimental campaign. The authors acknowledge access to the Durability and Characterisation (DURALAB) facility at Cardiff University (UK) that enabled part of the experiments presented in this work.

Data availability

Data is available on Zenodo (10.5281/zenodo.17210912).

References

Alahmad, S., Toumi, A., Verdier, J., François, R., 2009. Effect of crack opening on carbon dioxide penetration in cracked mortar samples. Mater. Struct. 42 (5), 559–566.
Ali, S.J.A., Rahmatabadi, D., Baghani, M., Baniassadi, M., 2024. Design, processing, 3D/4D printing, and characterization of the novel PETG–PBAT blends. J. Mater. Sci. 59 (20), 9150–9164. https://doi.org/10.1007/s10853-024-09761-8.
Ann, K.Y., et al., 2010. Service life prediction of a concrete bridge structure subjected to carbonation. Constr. Build. Mater. 24 (8), 1494–1501. https://doi.org/10.1016/j.conbuildmat.2010.01.023.
Audenaert, K., Marsavina, L., De Schutter, G., 2009. Influence of cracks on the service life of concrete structures in a marine environment. In: Key Engineering Materials. Trans Tech Publ. https://doi.org/10.4028/www.scientific.net/KEM.399.153.
Balzano, B., et al., 2021. Enhanced concrete crack closure with hybrid shape memory polymer tendons. Eng. Struct. 226, 111330. https://doi.org/10.1016/j.engstruct.2020.111330.
Cappellesso, V., et al., 2023. A review of the efficiency of self-healing concrete technologies for durable and sustainable concrete under realistic conditions. Int. Mater. Rev. 68 (5), 556–603. https://doi.org/10.1080/09506608.2022.2145747.
Cappellesso, V.G., et al., 2024. Self-healing concrete with a bacteria-based or crystalline admixture as healing agent to prevent chloride ingress and corrosion in a marine environment. Develop. Built Environ. 19, 100486. https://doi.org/10.1016/j.dibe.2024.100486.
Carević, V., Ignjatović, I., 2019. Influence of loading cracks on the carbonation resistance of RC elements. Constr. Build. Mater. 227, 116583. https://doi.org/10.1016/j.conbuildmat.2019.07.309.
Chen, W., et al., 2021. Evaluation of self-healing performance of a smart composite material (SMA-ECC). Constr. Build. Mater. 290, 123216. https://doi.org/10.1016/j.conbuildmat.2021.123216.
Davies, R., et al., 2018. Large scale application of self-healing concrete: design, construction, and testing. Front. Mater. 5–2018. https://doi.org/10.3389/fmats.2018.00051.
De Belie, N., et al., 2018. A review of self-healing concrete for damage management of structures. Adv. Mater. Interfac. 5 (17), 1800074. https://doi.org/10.1002/admi.201800074.
De Brabandere, L., et al., 2024. Comparative analysis of three different types of self-healing concrete via permeability testing and a quasi-steady-state chloride migration test. Constr. Build. Mater. 411, 134288. https://doi.org/10.1016/j.conbuildmat.2023.134288.
De Rooij, M., Van Tittelboom, K., De Belie, N., Schlangen, E., 2013. Self-healing phenomena in cement-based materials. State-of-the-art Rep. RILEM Tech. Comm. https://doi.org/10.1007/978-94-007-6624-2.
De Schutter, G., 1999. Quantification of the influence of cracks in concrete structures on carbonation and chloride penetration. Mag. Concr. Res. 51 (6), 427–435. https://doi.org/10.1680/macr.1999.51.6.427.
EN 12390-12, 2020. Testing Hardened Concrete - Part 12: Determination of the Carbonation Resistance of Concrete - Accelerated Carbonation Method.
EN 12617-4, 2002. Products and Systems for the Protection and Repair of Concrete Structures - Test Methods - Part 4: Determination of Shrinkage and Expansion.
EN 196-1, 2016. Methods of Testing Cement - Part 1. Determination of strength.
Commission, E.. The European green deal. Available from: https://commission.europa.eu/strategy-and-policy/priorities-2019-2024/european-green-deal_en.
Association, G.C.a.C., 2024. Cement Industry Net Zero Progress Report 2024/25.
Grosso Giordano, F., et al., 2024. Beyond the surface: coupling water permeability assessments to X-ray micro-computed tomography for evaluation of self-healing on lime-based mortars. Constr. Build. Mater. 431, 136603. https://doi.org/10.1016/j.conbuildmat.2024.136603.
Gruyaert, E., et al., 2016. Self-healing mortar with pH-sensitive superabsorbent polymers: testing of the sealing efficiency by water flow tests. Smart Mater. Struct. 25 (8), 084007. https://doi.org/10.1088/0964-1726/25/8/084007.
Gu, C.-p., Ye, G., Sun, W., 2015. A review of the chloride transport properties of cracked concrete: experiments and simulations. J. Zhejiang Univ. - Sci. 16 (2), 81–92.
Hamada, H.M., et al., 2023. Effect of silica fume on the properties of sustainable cement concrete. J. Mater. Res. Technol. 24, 8887–8908. https://doi.org/10.1016/j.jmrt.2023.05.147.
He, S., et al., Perspectives on the incorporation of self-healing in the design practice of reinforced concrete structures. Struct. Concr.https://doi.org/10.1002/suco.202401045.
He, S., et al., 2023. Distribution of porosity surrounding a microfiber in cement paste. Cement Concr. Compos. 142, 105188. https://doi.org/10.1016/j.cemconcomp.2023.105188.
Huang, L., et al., 2018. Carbon emission of global construction sector. Renew. Sustain. Energy Rev. 81, 1906–1916. https://doi.org/10.1016/j.rser.2017.06.001.
Ismail, M., Toumi, A., François, R., Gagné, R., 2008. Effect of crack opening on the local diffusion of chloride in cracked mortar samples. Cement Concr. Res. 38 (8), 1106–1111. https://doi.org/10.1016/j.cemconres.2008.03.009.
Jin, W., Yan, Y., Wang, H., 2010. *Chloride diffusion in the cracked concrete.* Fracture mechanics of concrete and concrete structures-assessment, Durability. Monitor. Retrofitt. 880–886.
Kim, M.-Y., Yang, E.-I., Yi, S.-T., 2013. Application of the colorimetric method to chloride diffusion evaluation in concrete structures. Constr. Build. Mater. 41, 239–245. https://doi.org/10.1016/j.conbuildmat.2012.11.084.
Maddalena, R., et al., 2020. A crack closure system for cementitious composite materials using knotted shape memory polymer (k-SMP) fibres. Cement Concr. Compos. 114, 103757. https://doi.org/10.1016/j.cemconcomp.2020.103757.

Maddalena, R., et al., 2022. Applications and life cycle assessment of shape memory polyethylene terephthalate in concrete for crack closure. Polymers 14 (5), 933. https://doi.org/10.3390/polym14050933.
Maddalena, R., Taha, H., Gardner, D., 2021. Self-healing potential of supplementary cementitious materials in cement mortars: sorptivity and pore structure. Develop. Built Environ. 6, 100044. https://doi.org/10.1016/j.dibe.2021.100044.
Marsavina, L., et al., 2009. Experimental and numerical determination of the chloride penetration in cracked concrete. Constr. Build. Mater. 23 (1), 264–274. https://doi.org/10.1016/j.conbuildmat.2007.12.015.
Mihashi, H., Nishiwaki, T., 2012. Development of engineered self-healing and self-repairing concrete-state-of-the-art report. J. Adv. Concr. Technol. 10 (5), 170–184. https://doi.org/10.3151/jact.10.170.
Rahmatabadi, D., et al., 2024. 4D printing and annealing of PETG composites reinforced with short carbon fibers. Phys. Scri. 99 (5), 055957. https://doi.org/10.1088/1402-4896/ad3b40.
Snoeck, D., et al., 2014. Self-healing cementitious materials by the combination of microfibres and superabsorbent polymers. J. Intell. Mater. Syst. Struct. 25 (1), 13–24. https://doi.org/10.1177/1045389X12438623.
Snoeck, D., De Belie, N., 2015. From straw in bricks to modern use of microfibers in cementitious composites for improved autogenous healing – a review. Constr. Build. Mater. 95, 774–787. https://doi.org/10.1016/j.conbuildmat.2015.07.018.
Song, H.-W., Kwon, S.-J., Byun, K.-J., Park, C.-K., 2006. Predicting carbonation in early-aged cracked concrete. Cement Concr. Res. 36 (5), 979–989. https://doi.org/10.1016/j.cemconres.2005.12.019.
Teall, O., et al., 2017. Development of high shrinkage polyethylene terephthalate (PET) shape memory polymer tendons for concrete crack closure. Smart Mater. Struct. 26 (4), 045006. https://doi.org/10.1088/1361-665X/aa5d66.
Torres, J., Andrade, C., 2014. Influence of crack width on long term degradation of concrete structures. In: Durability of Reinforced Concrete from Composition to Protection: Selected Papers of the 6th International RILEM Phd Workshop Held in Delft, the Netherlands, July 4-5, 2013. Springer. https://doi.org/10.1007/978-3-319-09921-7_9.
Tran, N.P., et al., 2022. Microstructural characterisation of cementitious composite incorporating polymeric fibre: a comprehensive review. Constr. Build. Mater. 335, 127497. https://doi.org/10.1016/j.conbuildmat.2022.127497.
Tziviloglou, E., Jonkers, H.M., Schlangen, E., 2014. Bacteria-based self-healing concrete to increase liquid tightness of cracks. In: First Conference on Ageing of Materials and Structures, pp. 650–655. Delft, The Netherlands.
Tziviloglou, E., Wiktor, V., Jonkers, H., Schlangen, E., 2016. Bacteria-based self-healing concrete to increase liquid tightness of cracks. Constr. Build. Mater. 122, 118–125. https://doi.org/10.1016/j.conbuildmat.2016.06.080.
Van Belleghem, B., Van den Heede, P., Van Tittelboom, K., De Belie, N., 2017. Quantification of the service life extension and environmental benefit of chloride exposed self-healing concrete. Materials 10 (1), 5. https://doi.org/10.3390/ma10010005.
Van den Heede, P., et al., 2018a. Screening of different encapsulated polymer-based healing agents for chloride exposed self-healing concrete using chloride migration tests. Key Eng. Mater. 761, 152–158. https://doi.org/10.4028/www.scientific.net/KEM.761.152.
Van den Heede, P., et al., 2018b. Screening encapsulated polymeric healing agents for carbonation-exposed self-healing concrete, service life extension, and environmental benefit. In: International Congress on Polymers in Concrete. Springer, Washington DC, USA.
Van Mullem, T., 2021. Development of Standard Testing Methods to Evaluate the self-healing Efficiency of Concrete. Ghent University.
Van Mullem, T., R. Caspeele, and N. De Belie. The influence of SAPs on chloride ingress in cracked concrete. in *Concrete Solutions 2019 – 7th International Conference on Concrete Repair* 2019. Cluj Napoca, Romania: EDP Sciences.https://doi.org/10.1051/matecconf/201928908007.
Van Mullem, T., et al., 2020a. Addressing the need for standardization of test methods for self-healing concrete: an inter-laboratory study on concrete with macrocapsules. Sci. Technol. Adv. Mater. 21 (1), 661–682. https://doi.org/10.1080/14686996.2020.1814117.
Van Mullem, T., et al., 2020b. Raw Data and Supplementary Material of the Fifth Inter-laboratory Testing Program (RRT5, self-healing Concrete with Macrocapsules) of the EU COST Action SARCOS. Zenodo. https://doi.org/10.5281/zenodo.3865635.
Van Mullem, T., et al., 2020d. Influence of crack geometry and crack width on carbonation of high-volume fly ash (HVFA) mortar. In: RILEM Spring Convention 2020. University of Minho, Guimarães, Portugal.
Van Mullem, T., et al., 2021. Influence of self-healing via embedded macrocapsules filled with polyurethane on carbonation of high-volume fly ash mortar. In: RILEM Annual Week. Springer, pp. 231–240.
Van Mullem, T., et al., 2024. Influence of superabsorbent polymers on the chloride ingress of mortar measured by chloride diffusion and a quasi-steady-state migration test. Cement Concr. Compos. 150, 105563. https://doi.org/10.1016/j.cemconcomp.2024.105563.
Van Mullem, T., Gruyaert, E., Caspeele, R., De Belie, N., 2020c. First large scale application with self-healing concrete in Belgium: analysis of the laboratory control tests. Materials 13 (4), 997. https://doi.org/10.3390/ma13040997.
Wang, Q., Yao, B., Lu, R., 2020. Behavior deterioration and microstructure change of polyvinyl alcohol fiber-reinforced cementitious composite (PVA-ECC) after exposure to elevated temperatures. Materials 13 (23), 5539. https://doi.org/10.3390/ma13235539.
Wang, X.-H., Val, D.V., Zheng, L., Jones, M.R., 2018. Influence of loading and cracks on carbonation of RC elements made of different concrete types. Constr. Build. Mater. 164, 12–28. https://doi.org/10.1016/j.conbuildmat.2017.12.142.
Xie, T., 2011. Recent advances in polymer shape memory. Polymer 52 (22), 4985–5000. https://doi.org/10.1016/j.polymer.2011.08.003.
Yang, Y., Lepech, M.D., Yang, E.-H., Li, V.C., 2009. Autogenous healing of engineered cementitious composites under wet–dry cycles. Cement Concr. Res. 39 (5), 382–390. https://doi.org/10.1016/j.cemconres.2009.01.013.
Yoon, I.-S., Schlangen, E., 2010. Long/short term experimental study on chloride penetration in cracked concrete. Key Eng. Mater. 417–418, 765–768. https://doi.org/10.4028/www.scientific.net/KEM.417-418.765.
Yoon, I.-S., Schlangen, E., 2014. Experimental examination on chloride penetration through micro-crack in concrete. KSCE J. Civ. Eng. 18 (1), 188–198.
Zhang, P., et al., 2022. Mechanical properties of polyvinyl alcohol fiber-reinforced cementitious composites after high-temperature exposure. Gels 8 (10), 662. https://doi.org/10.3390/gels8100662.
Zhang, S.P., Zong, L., Dong, L.F., Zhang, W., 2011. Influence of cracking on carbonation of cement-based materials. Adv. Mater. Res. 261–263, 84–88. https://doi.org/10.4028/www.scientific.net/AMR.261-263.84.